Biosensors and Bioelectronics 33 (2012) 204–210

Contents lists available at SciVerse ScienceDirect

Biosensors and Bioelectronics

journal homepage: www.elsevier.com/locate/bios

Inlaid Nd-substituted bismuth titanate nanoplates for protein immobilization and Nd-controlled electrochemical properties

Huan Guo[a,b,1], Cui Ye[b,1], Hanchang He[a], Zhiwu Chen[c], Jianqiang Hu[b,*], Guanqi Hu[b], Aiqing Li[a,**]

[a] Key Lab for Organ Failure Research, Ministry of Education of China, Nanfang Hospital, Southern Medical University, Guangzhou 510515, PR China
[b] Key Lab for Fuel Cell Technology of Guangdong Province, College of Chemistry and Chemical Engineering, South China University of Technology, Guangzhou 510640, PR China
[c] College of Materials Science and Engineering, South China University of Technology, Guangzhou 510640, PR China

ARTICLE INFO

Article history:
Received 18 October 2011
Received in revised form
13 December 2011
Accepted 28 December 2011
Available online 16 January 2012

Keywords:
$Bi_{4-x}Nd_xTi_3O_{12}$
Inlaid nanoplates
Direct electrochemistry
Hemoglobin
Hydrogen peroxide
Biosensor

ABSTRACT

Neodymium (Nd) substituted bismuth titanate ($Bi_{4-x}Nd_xTi_3O_{12}$, BNTO-*x*) nanoplates inlaid one another were prepared by sol–gel hydrothermal method, which was explored for protein immobilization and biosensor fabrication. Comparative experiments witnessed that Bi^{3+} ions in bismuth titanate ($Bi_4Ti_3O_{12}$, BTO) were successfully substituted with Nd^{3+} ions, and the electrochemical properties of the Hb–Chi–BNTO biosensors closely depended on the Nd^{3+} ion content. With increasing the Nd^{3+} doping content, the electrochemical performance of the Hb–Chi–BNTO-*x* biosensors showed regularly variable. Moreover, compared with the Hb–Chi–BTO and other Hb–Chi–BNTO-*x* biosensors, the Hb–Chi–BNTO-0.85 biosensor had more excellent electrochemical and electrocatalytic properties such as stronger redox peak currents (approximately three-fold), smaller peak-to-peak separation (50 mV), larger heterogeneous electron transfer rate ($14.1 \pm 3.8\ s^{-1}$), higher surface concentration of electroactive redox protein (about 8.16×10^{-11} mol/cm^2), and better reproducibility and stability. The Nd-depended electrochemical properties of the Hb–Chi–BNTO biosensors may open up a new idea for designing third-generation electrochemical biosensors, and the BNTO-0.85-based biosensor is also expected to find potential applications in many areas such as biomedical, food, and environmental detection.

1. Introduction

High-performance electrochemical biosensors are essential for uncovering and understanding the kinetics and thermodynamics of biological redox processes (Noell and Noell, 2011; Ahmadalinezhad and Chen, 2011; Wang et al., 2011), and exploiting their potential applications in medical diagnosis (Shi et al., 2007), pharmaceutical and environment controls (Moreau et al., 2008), enzyme biofuel cells (Zafar et al., 2009), and biodetection (Soleymani et al., 2009). To obtain high-performance electrochemical biosensors, it is of key importance to successfully immobilize a redox protein onto an electrode surface and form efficient electrical communication between the redox protein and the electrode while retaining the protein stability and bioactivity (Willner et al., 2007; Lu et al., 2009). Recent studies have indicated that inorganic nanomaterials are favorable hosts for protein entrapment due to their higher surface-volume ratio, more chemical active sites, better electron transfer carriers, and rigid framework (Chen et al., 2009a; Xie et al., 2010; Parra-Alfambra et al., 2011). It is well-known that electrochemical performances of nanomaterial-based biosensors closely associate with nanomaterials' components, sizes, structures, and shapes (Sahoo et al., 2011; Morita et al., 2011; Won et al., 2011). To design novel sensing systems and enhanced electrochemical performance of such biosensors, many efforts have been made to date by tailoring inorganic nanomaterials' components, sizes, structures, and shapes (Ye et al., 2010; Chirea et al., 2009; Zhang et al., 2011a; Feng et al., 2011; Ahmad et al., 2010; Hu et al., 2011). However, to the best of our knowledge, it is still rarely reported to fabricate high-performance electrochemical biosensors through partly substituting one element within multi-component inorganic nanocrystal with another component but still preserving its intrinsic crystalline structure.

Ferroelectric bismuth titanate ($Bi_4Ti_3O_{12}$, BTO), consisting of three TiO_6 octahedral layers with Bi at the A sites sandwiched between $[Bi_2O_2]^{2+}$ layers along the *c*-axis (Liang et al., 2008), has high Curie temperature, large spontaneous polarization, relatively low coercive field, low dielectric constant, and high electrical conductivity anisotropy properties (Scott and Araujo, 1989). But, regretfully, BTO suffers from poor fatigue endurance against a repeated switching of polarization states (Park et al., 2009), which is probably due to its lattice defects. It has been reported that Nd-substituted $Bi_4Ti_3O_{12}$ ($Bi_{4-x}Nd_xTi_3O_{12}$, BNTO-*x*), especially

* Corresponding author. Tel.: +86 20 222 36670; fax: +86 20 222 36670.
** Corresponding author. Tel.: +86 20 62787973; fax: +86 20 87281713.
E-mail addresses: jqhusc@scut.edu.cn (J. Hu), stephanie586@gmail.com (A. Li).
[1] Huan Guo and Cui Ye contributed equally to this work.

0956-5663/$ – see front matter © 2012 Elsevier B.V. All rights reserved.
doi:10.1016/j.bios.2011.12.054

$Bi_{3.15}Nd_{0.85}Ti_3O_{12}$ (BNTO-0.85), shows an excellent fatigue-free property with relatively large remanent polarization (Chon et al., 2002). Moreover, Lu's group has demonstrated that electrical properties of the BNTO crystals are highly dependent on the nature of the A cation (wherein A cation means Bi^{3+} or Nd^{3+} ions) (Liang et al., 2008). Recently, we have also successfully constructed a stable and high-performance electrochemical biosensor through encapsulating redox proteins into $Bi_4Ti_3O_{12}$ nanorods and nanosheets (Chen et al., 2009b). Gao's group indicated that Fe-substituted titania nanosheets-constructed biosensor had better electrochemical and electrocatalytic properties in comparison with titania nanosheets-constructed biosensor (Shi et al., 2009). Therefore, it is worth anticipating that Nd-substituted $Bi_4Ti_3O_{12}$ nanoplates, especially $Bi_{3.15}Nd_{0.85}Ti_3O_{12}$ nanoplates, can construct more promising electrochemical biosensors in comparison with similarly structured $Bi_4Ti_3O_{12}$ nanomaterials.

In the present study, inlaid $Bi_{4-x}Nd_xTi_3O_{12}$ nanoplates were synthesized by sol–gel hydrothermal method. Moreover, the BNTO nanoplates intercalated one another were utilized, together with hemoglobin (Hb) and chitosan (Chi), to fabricate novel electrochemical biosensors. With the aid of a multilayer Hb–Chi–BNTO-*x* composite film, Hb could retain its native structure and bioactivity well, and facilitated direct electron transfer of the Hb immobilized in the multilayer film has been acquired. Comparative studies revealed that the electrochemical properties of the BNTO-based biosensors deeply associated with the Nd^{3+} content, moreover, relative to the biosensor based on inlaid BTO and other BNTO-*x* nanoplates, the BNTO-0.85-based biosensor not only had stronger direct electron transfer capacity, but also displayed better electrocatalytic performance over a wider linear range, lower detection limit, higher sensitivity, and smaller Michaelis–Menton constant, along with better reproducibility and stability for the detection of H_2O_2.

2. Materials and methods

2.1. Materials

Hb (MW 64,500, from bovine blood) and Chi were purchased from Sigma–Aldrich. Neodymium nitrate ($Nd(NO)_3{\cdot}5H_2O$) was obtained from Shanghai Aladdin Chemical Reagent Company. Other chemical reagents such as bismuth nitrate ($Bi(NO_3)_3{\cdot}5H_2O$), tetrabutyl titanate ($Ti(OC_4H_9)_4$), lactic acid ($C_3H_6O_3$), potassium chloride (KCl), potassium bromide (KBr), potassium ferricyanide ($K_3[Fe(CN)_6]$), potassium ferrocyanide ($K_4[Fe(CN)_6]$), and hydrogen peroxide (H_2O_2) were obtained from Guangdong Guanghua Chemical Reagent Company. All above reagents are of analytical grade and used without further purification. All aqueous solutions were prepared with Milli-Q purified water (>18.0 MΩ cm).

2.2. Preparation of inlaid BTO and BNTO-x nanoplates

In a typical procedure for the synthesis of inlaid $Bi_{3.5}Nd_{0.5}Ti_3O_{12}$ (BNTO-0.5), $Bi_{3.4}Nd_{0.6}Ti_3O_{12}$ (BNTO-0.6), $Bi_{3.3}Nd_{0.7}Ti_3O_{12}$ (BNTO-0.7), $Bi_{3.15}Nd_{0.85}Ti_3O_{12}$ (BNTO-0.85), $Bi_{3.1}Nd_{0.9}Ti_3O_{12}$ (BNTO-0.9), and $Bi_{3.0}Nd_{1.0}Ti_3O_{12}$ (BNTO-1.0) nanoplates, 0.015 mol $Ti(OC_4H_9)_4$ and the 3.5:0.5, 3.4:0.6, 3.3:0.7, 3.15:0.85, 3.1:0.9, and 3.0:1.0 molar ratios of $Bi(NO_3)_3{\cdot}5H_2O$ and $Nd(NO_3)_3{\cdot}5H_2O$ were added into 4.5 mL lactic acid, respectively, and kept stirring for 2 h to form homogeneous solutions. The solutions were diluted with 50 mL ultrapure water and the pH values were adjusted to 2–4, respectively. Then, the diluted solutions were heated at 70 °C for 3 h to obtain dry gels. Finally, the gels were added into 3 M NaOH solutions to form suspensions and were poured into three Teflon-lined stainless steel autoclaves with a filling capacity of 80%, respectively. The final products were obtained by heating the autoclaves at 180 °C for 48 h, repeatedly washing with Milli-Q water, and drying at 80 °C.

Inlaid BTO nanoplates were prepared using the same procedure except without $Nd(NO_3)_3{\cdot}5H_2O$.

2.3. Preparation of Hb–Chi–BTO and Hb–Chi–BNTO-x modified electrodes

The modified electrodes were prepared by a simple casting method. 3.0 mg/mL BTO and BNTO-*x* suspension solutions were first obtained by dispersing 3.0 mg BTO and BNTO-*x* powders in 1.0 mL ultrapure water and ultrasonically dispersing for 30 min, respectively. Then, equal volumes of 3 mg/mL BTO or BNTO-*x* solutions, 6 mg/mL Hb PBS, and 4.5 mg/mL Chi acetic acid solution (2 wt%) were mixed, respectively. Finally, 6 μL of the mixtures were cast onto the freshly prepared bare glass carbon (GC) electrodes to form uniform film electrodes, respectively. The dried electrodes were stored at 4 °C in 20 mM pH 7.0 PBS when not in use.

2.4. Apparatus and measurements

Scanning electron microscopy (SEM) and energy-dispersive X-ray spectroscopy (EDS) were performed with a field-emission microscope (LEO, 1530 VP) operated at an accelerating voltage of 30 kV. Powder X-ray diffraction (XRD) pattern was recorded on a powder sample using a D_{max}-IIIA (Japan) X-ray diffractometer with Cu Kα radiation (λ = 1.5418 Å). UV–visible (UV–vis) absorption spectroscopy measurement was carried out with a U-3010 spectrophotometer (Hitachi, Japan). The UV–vis samples were prepared by casting, respectively, Hb, Hb–Chi, Hb–Chi–BTO, and Hb–Chi–BNTO-0.85 solutions onto quartz glass slides and letting them dry naturally in air. Fourier-transform infrared (FTIR) spectra were obtained on Tensor 27 (Bruker Company, German). The FTIR samples were prepared according to the following procedure: Hb, Hb–Chi, Hb–Chi–BTO, and Hb–Chi–BNTO-0.85 solutions were first cast onto glass slides, respectively. Then, the glass slides were naturally dried in air. Finally, the dry films adhered to the glass slides were stripped off and tableted with KBr powder for FTIR measurement. Electrochemical experiments were performed at room temperature using a CHI 660 electrochemical workstation (CH Instruments, Inc., Austin, USA). All electrochemical measurements were based on a three-electrode system with the prepared modified electrode as working electrode, an Ag/AgCl (3 M KCl) electrode as reference electrode, and a platinum wire as auxiliary electrode.

3. Results and discussions

3.1. Morphology and structure characterization of the BTO and BNTO-x nanoplates

From representative SEM images of the as-prepared BTO and BNTO-0.85 (Fig. 1A and B), it could be clearly seen that both BTO and BNTO-0.85 had a well-defined three-dimensional (3D) structure and consisted of many nanoplates intercalated one another. The inlaid nanoplates easily formed a lot of cavities and porous structures and had high surface area and highly active sites, which were much useful for proteins to sequester in the cavities or bind on the surface. The thickness and side lengths of the inlaid BTO and BNTO-0.85 nanoplates were about 50 and 25 nm and 200 and 140 nm, respectively. Compared with the BTO, the BNTO-0.85 constructed by the smaller sizes should have higher surface area and more active sites, which was probably because the substitutions of Nd^{3+} ion with smaller ionic radius resulted in the uniformity increase of the preferred orientation of the crystal (Zhong et al., 2005). EDS spectra of the as-prepared BTO and BNTO-0.85 are shown in Fig. 1C and

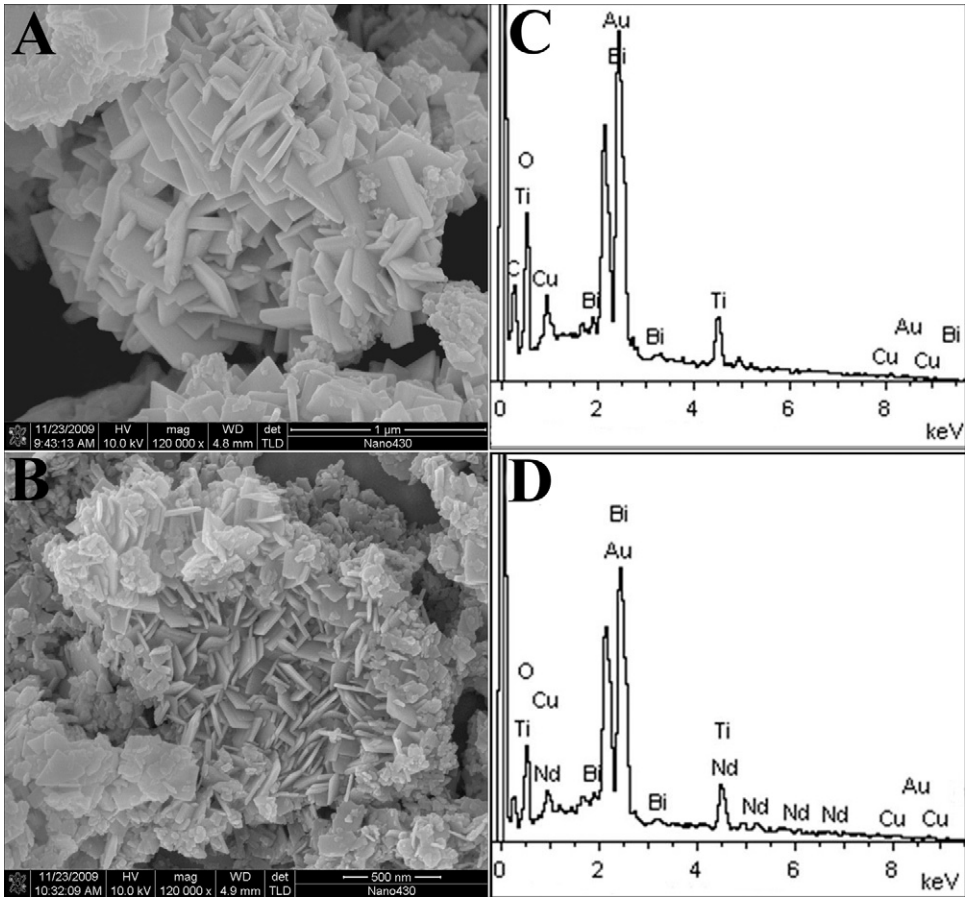

Fig. 1. (A, B) SEM images and (C, D) EDS spectra of inlaid BTO and BNTO-0.85 nanoplateds prepared using the present method, respectively. Scale bar: (A) 1 μm and (B) 500 nm.

D, respectively. The Cu, C, and Au elements were from the copper grids and spurted Au made for the SEM samples. The appearance of Bi, Ti, and O elements (Fig. 1C) indicated that the BTO was perhaps formed. Compared with Fig. 1C, Fig. 1D presented a new Nd element, suggesting that the Nd^{3+} ions were perhaps incorporated into the lattice of the BTO through partly substituting Bi^{3+} ions to form the BNTO-0.85 product.

To further confirm the formation of the inlaid BTO and BNTO-*x* nanoplates, XRD measurements were performed. Fig. S1 gives XRD patterns of the as-prepared BTO and BNTO-*x* nanoplates, respectively. It was important to note that all diffraction peaks of patterns b–d were completely consistent with those of pattern a. All the diffraction peaks of 21.5°, 23.3°, 27.1°, 30.1°, 32.9°, 37.1°, 38.5°, 39.7°, 47.3°, 51.5°, 57.1°, 62.7°, 64.3°, 69.6°, 77.2°, and 78.6° could be indexed to (0 8 0), (1 1 1), (0 10 0), (1 7 1), (2 0 0), (0 6 2), (0 14 0), (2 8 0), (2 0 2), (0 14 2), (1 7 3), (1 11 3), (1 2 13), (3 15 1), (3 7 3), and (1 19 3) planes of the orthorhohbic structure of bismuth titanate (JCPDS: 35-0795), respectively, demonstrating that the samples prepared using the sol–gel hydrothermal method were pure BTO or BNTO. The XRD patterns b–d in Fig. S1 displayed that no secondary phase was formed, which documented that partly Bi^{3+} ions were successfully substituted by Nd^{3+} ions and BTO and BNTO-*x* had the same crystal structure.

3.2. UV–vis and FTIR spectroscopic characterizations of the Hb–Chi–BTO and Hb–Chi–BNTO-x composite films

UV–vis absorption spectroscopy is usually employed to characterize the conformational change of heme protein and thus probe their possible denaturation because it can monitor possible changes of the Soret absorption band in the heme group (Xiao et al., 2009). Fig. 2A shows UV–vis absorption spectra of dry Hb, Hb–Chi, Hb–Chi–BTO, and Hb–Chi–BNTO-*x* films. An obvious UV–vis absorption peak at around 408 nm from dry Hb film could be clearly discerned, which is a characteristic Soret absorption band (curve a, Yue et al., 2011). When Hb was entrapped in the Chi film, the position of the Hb spectrum peak was similar to that of pure Hb film although its intensity slightly weakens (curve b). Moreover, compared with the Hb–Chi film, both peak position and intensity of the Hb entrapped in Hb–Chi–BTO (curve c) and Hb–Chi–BNTO-*x* (curve d) were nearly similar, suggesting that the Hb retained the essential features of its native secondary structure in the Hb–Chi–BTO and Hb–Chi–BNTO-*x* composite films and had good biocompatibility with the BTO and BNTO-*x*.

It is well known that the shapes and positions of the amide I (1700–1600 cm^{-1}) and amide II (1600–1500 cm^{-1}) infrared transmission bands of proteins can provide detailed information on the secondary structure of polypeptide chain of the proteins (Kauppinen et al., 1981). FTIR spectra of dry Hb, Hb–Chi, Hb–Chi–BTO, and Hb–Chi–BNTO-*x* composite films (Fig. 2B) showed that the spectra of amide I and II bands of Hb in Hb–Chi–BTO and Hb–Chi–BNTO-*x* composite films were nearly the same as those obtained for native Hb and Hb–Chi. The similarities of the spectra further suggested that the Hb retained the essential feature of its native secondary structure in the Hb–Chi–BTO and Hb–Chi–BNTO-*x* films and had good biocompatibility with the BTO and BNTO-*x*. The good biocompability of Hb entrapped in the BTO and BNTO-*x* could perhaps be attributed to its rigid framework and

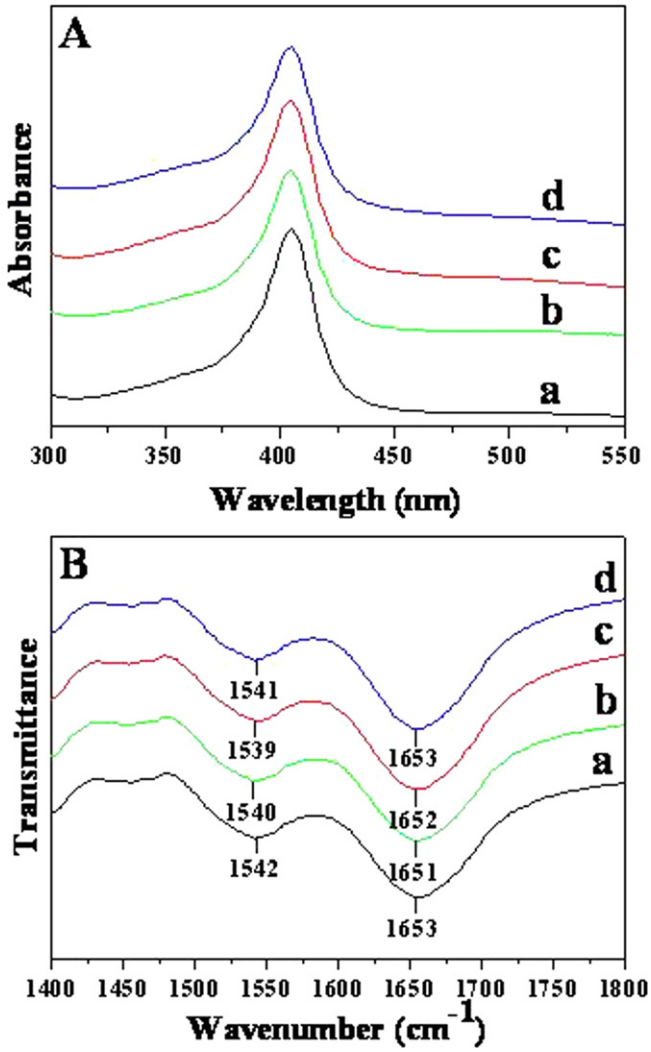

Fig. 2. (A) UV–vis absorption and (B) FTIR spectra of dry (a) Hb, (b) Hb–Chi, (c) Hb–Chi–BTO, and (d) Hb–Chi–BNTO-*x* films.

high chemical activity, which was available to hide or bind Hb and thus restrained its conformational change and unfolding.

3.3. Direct electron transfer of the modified electrodes

Fig. 3 gives representative cyclic voltammograms of different modified electrodes in 20 mM pH 7.0 PBS at the scan rate of 0.2 V/s. No redox peaks were observed at the Chi–BNTO-0.85/GC electrode (Fig. 3a), indicating that the Chi and BNTO-0.85 were not electroactive materials in the potential range. Nevertheless, the Hb–Chi–BTO (Fig. 3b) and Hb–Chi–BNTO-*x* (Fig. 3c–e) electrodes displayed a pair of well-defined and nearly reversible redox peaks of Hb for the Hb(Fe^{III})/Hb(Fe^{II}) redox couple transformation, which could be attributed to the direct electron transfer between the Hb and the underlying electrodes. It could be clearly seen from Fig. 3 that the electrochemical properties of the BNTO-*x*-based biosensors showed a regular change with increasing Nd^{3+} ion doping content. With the increase of the Nd^{3+} doping content from 0.0 to 0.85, the peak current intensity of the BNTO-*x*-based biosensor gradually increased. When the Nd doping was 0.85, the BNTO-0.85-based biosensor had the strongest peak intensity. However, further increasing the Nd^{3+} doping content, e.g., 0.9 and 1.0, its peak current intensity would decrease (Fig. S2). The strongest peak intensity of the 0.85 Nd doping was perhaps attributed to the lowest lattice

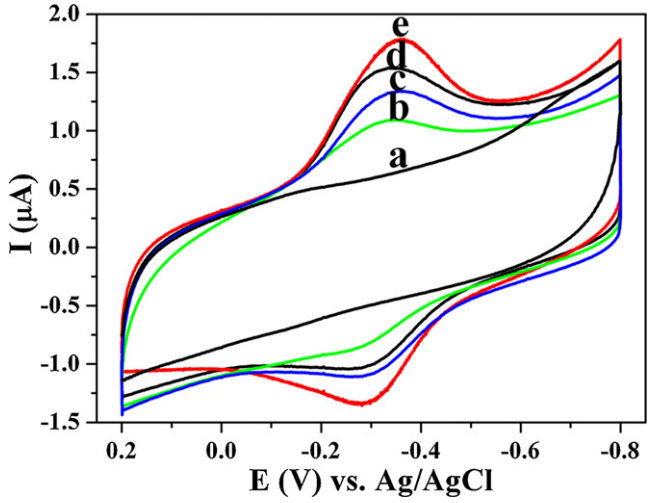

Fig. 3. Cyclic voltammograms of (a) Chi–BNTO-0.85/GC, (b) Hb–Chi–BTO/GC, (c) Hb–Chi–BNTO-0.5/GC, (d) Hb–Chi–BNTO-1.0/GC, and Hb–Chi–BNTO-0.85/GC electrodes in 20 mM pH 7.0 PBS with the scan rate of 0.2 V/s.

distortion of the BNTO-0.85 nanocrystals and thus resulted in the most effective tunnel for the electron transfer between the Hb and the underlying electrode. The apparent formal potential $E^{\circ\prime}$ of the Hb at the Hb–Chi–BNTO-0.85/GC electrode was about −0.32 V (vs. Ag/AgCl), a characteristic of Hb($Fe^{II/III}$) redox couples in composite films (Chen et al., 2009b; Lu et al., 2009). The $E^{\circ\prime}$ was very close to that (−0.345 V) gained from the Hb immobilized on nanosheet-based ZnO microspheres (Lu et al., 2008). Especially interestingly, compared with the BTO-based and other BNTO-based biosensors, the BNTO-0.85-based biosensor had stronger peak currents (about three times) and smaller peak-to-peak separation (ΔE_p, 50 and 60 mV for the BNTO- and BTO-based biosensors, respectively), revealing that the BNTO-0.85-based biosensor had faster and more quasi-reversible electron transfer process than the BTO-based and other BNTO-based biosensors. Moreover, Fig. 3 also suggested that Nd^{3+} doping content played an important role in the electrochemical properties of the BTO-based biosensors.

Using Faraday's law, $Q = nFA\Gamma^*$ (Q, n, F, A, and Γ^* represent the quantity of charge, the number of electron transferred, Faraday constant, effective electrode area, and surface average concentration of electroactive redox protein, respectively), the Γ^* of the electroactive Hb in the Hb–Chi–BNTO-0.85 film was estimated to be about 8.2×10^{-11} mol/cm^2 (assuming a one-electron transfer reaction), which was three-fold higher than that in the Hb–Chi–BTO film (about 2.5×10^{-11} mol/cm^2) and four-fold higher than that of the theoretical monolayer coverage (about 1.9×10^{-11} mol/cm^2) (Wang, 2005). The total amount of adsorbed Hb (Γ) was about 2.6×10^{-9} mol/cm^2, indicating that the electroactive Hb in the Hb–Chi–BNTO-0.85 film was about 3.2% of the total Hb content deposited on the electrode, which was much higher than those of Hb–$Co_xFe_{3-x}O_4$–chitosan and Hb–poly(lactic-co-glycolic acid)–ILs composite films (Yang et al., 2011; Zhang et al., 2011b). To sum up, BNTO-0.85 offered significant advantages over BTO and other immobilization films in facilitating direct electron transfer of redox proteins. Moreover, it should be noted that only difference between BTO and BNTO-0.85 was Nd^{3+} doping content, that is to say, Nd^{3+} doping played a decisive role in the enhanced electrochemical performance of the BTO-based biosensor. This could be perhaps explained by considering that Nd substitution greatly lowered the lattice stress and the ion displacement of A sites in the pervoskite layer in which Bi^{3+} strongly deviated from the center of the 12 coordinated sites in BTO (Liang et al., 2008). The decreased lattice distortion caused by Nd substitution would be available to offer

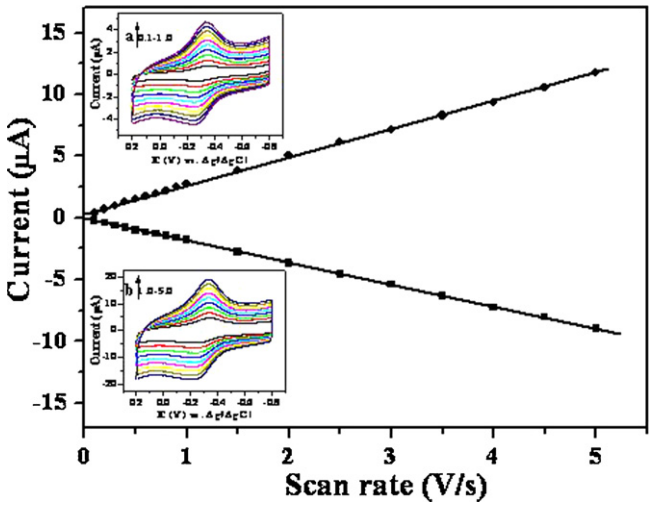

Fig. 4. Plots of oxidation peak currents and reduction peak currents versus scan rates for the Hb–Chi–BNTO-0.85 electrode. Scan rates: 0.1, 0.2, 0.3, 0.4, 0.5, 0.6, 0.7, 0.8, 0.9, 1.0 V/s (Inset a) and 1.5, 2.0, 2.5, 3.0, 3.5, 4.0, 4.5, 5.0 V/s (Inset b).

effective tunnel for the electron transfer between the Hb and the underlying electrode.

Cyclic voltammograms of Hb–Chi–BNTO-0.85/GC electrode scanned at low and high scan rates are shown in Fig. 4. As shown, both reduction and oxidation peak currents increased linearly with scan rates from 0.1 to 5.0 V/s. This result demonstrated that the BNTO-0.85 provided a friendly microenvironment for the intercalated Hb to maintain its activity to a great extent and it was a surface-confined electrochemical process. According to the Laviron method (Laviron, 1979), the apparent heterogeneous electron transfer rate constant (k_s) of the Hb immobilized on the Hb–Chi–BNTO-0.85/GC was estimated:

$$\log\frac{k_s}{s^{-1}} = \alpha\log(1-\alpha) + (1-\alpha)\log\alpha - \log\left[\left(\frac{RT/nF\upsilon}{s}\right)\right] - \frac{\alpha(1-\alpha)nF\Delta Ep}{2.3RT}$$

where α, k_s, ΔEp, n, R, T, and υ mean charge transfer coefficient, heterogeneous electron-transfer rate constant, peak separation, the number of electrons transferred, gas constant, absolute temperature, and scan rate, respectively. By taking α as 0.5 and $\upsilon > 0.2$ V/s, the average k_s was determined to be about $14.1 \pm 3.8\ s^{-1}$, which was larger than that of the Hb immobilized on Hb–Chi–BTO/GC ($11.9 \pm 3.2\ s^{-1}$) and much larger than those of the Hb immobilized on Hb–Nafion–GMC/GC ($1.20\ s^{-1}$, Lu et al., 2009) and Hb–Nafion–CNTs/GC ($2.54\ s^{-1}$, George and Lee, 2009), suggesting that the BNTO-0.85-based biosensor had a faster electron transfer process in comparison with the BTO-based biosensor.

The influence of the solution pH on the electrochemistry behavior of Hb at the Hb–Chi–BNTO-0.85 electrode was also evaluated. Fig. S3 gives cyclic voltammograms of the Hb–Chi–BNTO-0.85 electrode in the solutions with different pH values. Stable and well-defined cyclic voltammograms could be observed in the pH range of 5.0–9.0. With increasing pH from 5.0 to 9.0, both the reduction and oxidation peaks shifted linearly to the negative (Fig. S4). All the voltammetric peak potentials switched among the pH values were reversible. The slope from the linear plot of $E^{\circ\prime}$ versus pH was about −53.3 mV/pH, which was close to the theoretical value of −58.0 mV/pH for a single proton transfer coupled to a reversible single electron transfer. Therefore, the reaction could be represented as follows:

$$Hb[Heme(Fe^{III})] + H^+ + e^- \leftrightarrow Hb[Heme(Fe^{II})]$$

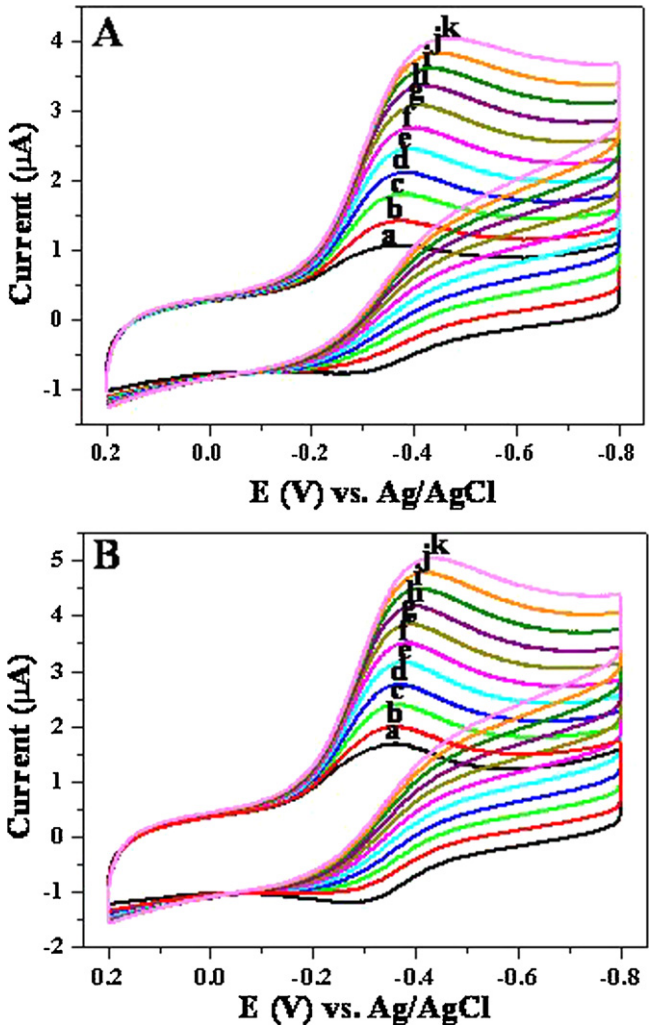

Fig. 5. Electrocatalysis of the (A) Hb–Chi–BTO and (B) Hb–Chi–BNTO-0.85 biosensors towards H_2O_2 in PBS with the scan rate of 0.2 V/s and H_2O_2 concentrations of (a) 0, (b) 60, (c) 120, (d) 180, (e) 240, (f) 300, (g) 360, (h) 420, (i) 480, (j) 540, and (k) 600 μM.

3.4. Electrocatalytic property of the Hb–Chi–BNTO-0.85/GC electrode

To evaluate and compare electrocatalytic property of the Hb entrapped on inlaid BNTO-0.85 nanoplates, the cyclic voltammetry of the Hb–Chi–BNTO-0.85/GC electrode towards H_2O_2 was investigated by comparing with the Hb–Chi–BTO/GC electrode. Fig. 5 records cyclic voltammograms of the Hb–Chi–BNTO-0.85/GC and Hb–Chi–BTO/GC electrodes in the PBS containing different H_2O_2 concentrations in the absence of oxygen. With the addition of H_2O_2, the reduction peak currents (about −0.36 V) of both Hb–Chi–BNTO-0.85/GC and Hb–Chi–BTO/GC electrodes dramatically increased with the gradual decrease and even disappearance of the oxidation peak, suggesting an occurrence of electrocatalytic reduction of H_2O_2 for both the Hb–Chi–BNTO-0.85/GC and Hb–Chi–BTO/GC electrodes. Moreover, it was easily inferred from Fig. 5 that the Hb–Chi–BNTO-0.85 electrode had larger reduction peak current under the same H_2O_2 concentration than the Hb–Chi–BTO electrode, revealing that the BNTO-0.85-based biosensor possessed more excellent electrocatalytic property in comparison with the BTO-based biosensor. In addition, Fig. 5 indicated that the reduction peak potentials of both Hb–Chi–BNTO-0.85/GC and

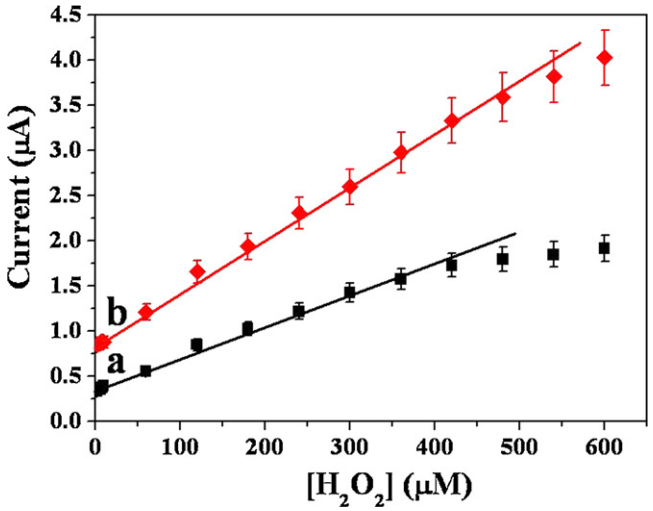

Fig. 6. Plot of electrocatalytic currents versus H_2O_2 concentrations for the (a) Hb–Chi–BTO/GC and (b) Hb–Chi–BNTO-0.85/GC electrodes in PBS.

Hb–Chi–BTO/GC electrodes shifted negatively with the gradual increase of H_2O_2, which could be ascribed to the different electrode reaction kinetics of different H_2O_2 concentrations. Above results (Fig. 4) have demonstrated that the electrode reaction of the BNTO-0.85-based biosensor was a surface-confined electrochemical process. Therefore, with increasing H_2O_2 concentrations, H_2O_2 was more difficult to completely diffuse into the electrode surface, which resulted in the requirement of more negative potential for the H_2O_2 catalysis (Mazzei et al., 2009).

As shown in Fig. 6, the linear range of the BNTO-0.85-based biosensor for the detection of H_2O_2 (Fig. 6b) was from 2.0×10^{-6} to 5.3×10^{-4} M ($R = 0.999$, $n = 20$), which was much wider than that (from 2.0×10^{-6} to 4.0×10^{-4} M) of the BTO-based biosensor (Fig. 6a) and other reported values (Lu et al., 2008; Wu et al., 2011). The detection limit of H_2O_2 at the Hb–Chi–BNTO-0.85 electrode was 4.2×10^{-7} M when signal-to-noise ratio (S/N) was 3, which was lower than that (7.4×10^{-7} M) of the Hb–Chi–BTO electrode. The sensitivity of the Hb–Chi–BNTO-0.85 electrode was calculated to be about 83 mA cm^{-2} M^{-1}, which was much larger than that (50 mA cm^{-2} M^{-1}) of the Hb–Chi–BTO electrode. These indicated that the Nd doping greatly improved electrocatalytic activity of the BTO-based biosensor towards H_2O_2.

At higher H_2O_2 concentrations, the plots tended to level off, which were characteristics of redox protein-based catalysis (Jena and Raj, 2011). The apparent Michaelis–Menton constant (K_M^{app}) could be estimated according to the Lineweaver–Burk equation (Kamin and Wilson, 1980):

$$I_{ss}^{-1} = I_{max}^{-1} + K_M^{app} C^{-1} I_{max}^{-1}$$

where I_{ss}, I_{max}, and C stand for the steady-state response current after the addition of substrate, the maximum current measured under saturated substrate condition, and the bulk concentration of the substrate. In the BNTO-0.85-based biosensor, K_M^{app} was estimated to be about 103 μM, which was much smaller than that (175 μM) of the BTO-based biosensor and others reported (Zeng et al., 2010). The relatively small K_M^{app} indicated that the BNTO-0.85-based biosensor had high catalytic efficiency to the reduction of H_2O_2.

3.5. Reproducibility and stability of the modified electrodes

The reproducibility and stability of the modified electrodes were also evaluated by cyclic voltammetry. The relative standard deviations of the BTO- and BNTO-0.85-based biosensors response to 120 μM H_2O_2 for seven successive measurements were 4.6% and 3.1%, respectively, suggesting good reproducibility. To investigate electrode-to-electrode reproducibility of the BTO- and BNTO-0.85-based biosensors, seven biosensors were fabricated independently under the same conditions. The relative standard deviations of the BTO- and BNTO-0.85-based biosensors were 9.0% and 5.8%, respectively, indicating accepted electrode-to-electrode reproducibility.

By comparing the cyclic voltammetric peak currents of the Hb entrapped in BTO and BNTO-0.85 with time intervals of 4 h, the biosensor stabilities were studied. The decrease of the cathodic peak currents of the BTO-based and BNTO-0.85-based biosensors immersed in PBS for 4 h were less than 4.7% and 2.4%, respectively, revealing that the biosensors possessed good stability. Moreover, the BTO-based and BNTO-0.85-based biosensors could retain 93.3% and 95.8% of their initial responses after three-week storage, suggesting good long-term stability. To sum up, the BTO- and BNTO-0.85-based biosensors had good reproducibility and stability. Moreover, the BNTO-0.85-based biosensor possessed better reproducibility and stability in comparison with the BTO-based biosensor, which could be ascribed to the following advantages: (1) the BNTO-0.85 nanoplates showed an excellent fatigue-free property with relatively large remanent polarization; (2) the Nd substitution lowered the lattice defect and the ion displacement of A sites in the pervoskite layer in which Bi^{3+} strongly deviated from the center of the 12 coordinated sites in BTO; (3) the decreased lattice distortion caused by Nd substitution would be available for proteins to sequester in the cavities or bind on the surface and build an effective tunnel for the electron transfer between the Hb and the BNTO-0.85-based electrode.

4. Conclusions

In summary, we have successfully synthesized inlaid $Bi_{3.15}Nd_{0.85}Ti_3O_{12}$ nanoplates by sol–gel hydrothermal method, using which a novel H_2O_2 biosensor was constructed through combining Chi and Hb. The underlying results disclosed that Nd^{3+} ions successfully substituted for partial Bi^{3+} ions into BTO layered structure. Comparative studies demonstrated that the BNTO-*x*-based biosensors had more excellent electrochemical performance and showed regularly variable in comparison with the Hb–Chi–BTO. Especially, the Hb–Chi–BNTO-0.85 biosensor had more excellent electrochemical and electrocatalytic properties such as stronger redox peak currents, smaller peak-to-peak separation, larger heterogeneous electron transfer rate, higher surface concentration of electroactive redox protein, and better reproducibility and stability. This indicated that the Nd^{3+} doping greatly improved the electrochemical properties of the layered pervoskite BTO, which presented a new idea for designing high-performance electrochemical biosensors through substituting original component with new component while keeping original crystal structure. Moreover, the BNTO-0.85-based biosensor may find potential applications in biomedical, food, and environmental detection.

Acknowledgements

The work was financially supported by the National Natural Science Foundation of China (No. 21173087), the Research Fund for the Doctoral Program (New Young Teacher) of Higher Education of China (Grant No. 20104433120005) and the Natural Science Foundation of Guangdong Province, China (Grant No. 10451051501005757), and Specialized Fund for Talent Introduction in Higher Education Institutions in Guangdong to A.Q. Li (No. 343).

Appendix A. Supplementary data

Supplementary data associated with this article can be found, in the online version, at doi:10.1016/j.bios.2011.12.054.

References

Ahmad, M., Pan, C.F., Zhu, J., 2010. J. Mater. Chem. 20, 7169.
Ahmadalinezhad, A., Chen, A.C., 2011. Biosens. Bioelectron. 26, 4508.
Chen, X.H., Hu, J.Q., Chen, Z.W., Feng, X.M., Li, A.Q., 2009a. Biosens. Bioelectron. 24, 3448.
Chen, Z.W., Yu, Y., Guo, H., Hu, J.Q., 2009b. J. Phys. D: Appl. Phys. 42, 125307.
Chirea, M., Cruz, A., Pereira, C.M., Silva, A.F., 2009. J. Phys. Chem. C 113, 13077.
Chon, U., Jang, H.M., Kim, M.G., Chang, C.H., 2002. Phys. Rev. Lett. 89, 087601.
Feng, X.M., Ruan, F.X., Hong, R.J., Ye, J.S., Hu, J.Q., Hu, G.Q., Yang, Z.L., 2011. Langmuir 27, 2204.
George, S., Lee, H.K., 2009. J. Phys. Chem. B 113, 15445.
Hu, J.Q., Yu, Y., Guo, H., Chen, Z.W., Li, A.Q., Feng, X.M., Xi, B.M., Hu, G.Q., 2011. J. Mater. Chem. 21, 5353.
Jena, B.K., Raj, C.R., 2011. Biosens. Bioelectron. 26, 2960.
Kamin, R.A., Wilson, G.S., 1980. Anal. Chem. 52, 1198.
Kauppinen, J.K., Moffate, D.J., Mantsch, H.H., Cameron, D.G., 1981. Appl. Spectrosc. 35, 271.
Laviron, E., 1979. J. Electroanal. Chem. 101, 19.
Liang, K., He, X.Q., Qi, Y.J., Lu, C.J., 2008. J. Cryst. Growth 310, 2471.
Lu, X.B., Zhou, J.H., Lu, W., Liu, Q., Li, J.H., 2008. Biosens. Bioelectron. 23, 1236.
Lu, X.B., Xiao, Y., Lei, Z.B., Chen, J.P., 2009. Biosens. Bioelectron. 25, 244.
Mazzei, F., Favero, G., Frasconi, M., Tata, A., Pepi, F., 2009. Chem. Eur. J. 15, 7359.
Moreau, C.J., Dupuis, J.P., Revilloud, J., Arumugam, K., Vivaudou, M., 2008. Nat. Nanotechnol. 3, 620.
Morita, Y., Yoshida, W., Savory, N., Han, S.W., Tera, M., Nagasawa, K., Nakamura, C., Sode, K., Ikebukuro, K., 2011. Biosens. Bioelectron. 26, 4837.
Noell, T., Noell, G., 2011. Chem. Soc. Rev. 40, 3564.
Park, H.H., Lee, H.S., Park, H.H., Hill, R.H., Hwang, Y.T., 2009. J. Ceram. Soc. Jpn. 117, 604.
Parra-Alfambra, A.M., Casero, E., Petit-Dominguez, M.D., Barbadillo, M., Pariente, F., Vazquez, L., Lorenzo, E., 2011. Analyst 136, 340.
Sahoo, S., Husale, S., Karna, S., Nayak, S.K., Ajayan, P.M., 2011. J. Am. Chem. Soc. 133, 4005.
Scott, J.F., Araujo, C.A., 1989. Science 246, 1400.
Shi, H.B., Xia, T., Nel, A.E., Yeh, J.I., 2007. Nanomedicine 2, 599.
Shi, L.P., Gao, Q.M., Wu, Y.H., Chen, Z., Liu, A.R., 2009. Biosens. Bioelectron. 25, 948.
Soleymani, L., Fang, Z.C., Sargent, E.H., Kelley, S.O., 2009. Nat. Nanotechnol. 4, 844.
Wang, J., 2005. Analyst 130, 421.
Wang, X.X., Yang, T., Li, X.A., Jiao, K., 2011. Biosens. Bioelectron. 26, 2953.
Willner, I., Willner, B., Katz, E., 2007. Bioelectrochemistry 70, 2.
Won, Y.H., Huh, K., Stanciu, L.A., 2011. Biosens. Bioelectron. 26, 4514.
Wu, P., Cai, Z.W., Chen, J., Zhang, H., Cai, C.X., 2011. Biosens. Bioelectron. 26, 4012.
Xiao, X.L., Luan, Q.F., Yao, X., Zhou, K.B., 2009. Biosens. Bioelectron. 24, 2447.
Xie, J.S., Feng, X.M., Hu, J.Q., Chen, X.H., Li, A.Q., 2010. Biosens. Bioelectron. 25, 1186.
Yang, W.Y., Zhou, X., Zheng, N., Li, X.J., Yuan, Z.B., 2011. Electrochim. Acta 56, 6588.
Ye, C., Kong, Q.C., Wu, R., Hu, J.Q., Chen, Z.W., Li, A.Q., 2010. Mater. Lett. 64, 1720.
Yue, R., Lu, Q., Zhou, Y.K., 2011. Biosens. Bioelectron. 26, 4436.
Zafar, M.N., Tasca, F., Gorton, L., Patridge, E.V., Ferry, J.G., Noll, G., 2009. Anal. Chem. 81, 4082.
Zeng, Q., Cheng, J.S., Tang, L.H., Liu, X.F., Liu, Y.Z., Li, J.H., Jiang, J.H., 2010. Adv. Funct. Mater. 20, 3366.
Zhang, Q., Wu, S.Y., Zhang, L., Lu, J., Verproot, F., Liu, Y., Xing, Z.Q., Li, J.H., Song, X.M., 2011a. Biosens. Bioelectron. 26, 2632.
Zhang, Y., Sun, X.M., Jia, N.Q., 2011b. Sens. Actuators B Chem. 157, 527.
Zhong, X.L., Wang, J.B., Zhou, Y.C., Liu, J.J., Zheng, X.J., 2005. J. Cryst. Growth 277, 233.